

Electrochemically Assisted Deposition as a New Route to Transparent Conductive Indium Tin Oxide Films

Nina I. Kovtyukhova* and Thomas E. Mallouk*

Department of Chemistry, The Pennsylvania State University, University Park, Pennsylvania 16802

Received June 5, 2010. Revised Manuscript Received July 26, 2010

Tin-doped indium oxide (ITO) films with Sn/In atomic ratios in the range 0–0.1 were synthesized by electrochemically assisted deposition (EAD). The process involves a fast one-step cathodic deposition of a highly crystalline In–Sn hydroxide (InSnOH) film followed by thermal conversion into ITO at 300 °C. The cathodic precipitation of InSnOH is preceded by formation of an In–Sn complex in solution. The films were characterized by field emission scanning electron microscopy, X-ray photoelectron spectroscopy, X-ray diffraction, UV–visible spectroscopy, and electrical measurements. In the Sn/In atomic ratio range 0–0.1, InSnOH and ITO films adopt the morphologies and cubic crystal structures of In(OH)₃ and In₂O₃, respectively. The atomic environment of Sn and O atoms in the ITO films was shown to resemble that of films deposited by other techniques and commercial ITO samples made by chemical vapor deposition. Separate tin oxide/hydroxide phases were not observed by any of the characterization methods. The morphology of the EAD ITO films consists of submicrometer-size bundles of parallel thin nanorods as the major structural blocks. The orientation of these bundles strongly affects the electronic conductivity of the film. The resistance of the EAD ITO films decreases by more than 2 orders of magnitude as the Sn/In atomic ratio increases from 0 to 0.1. After heating in air at 600 °C, 200–300 nm thick EAD ITO films show visible transmission of about 84% and resistivity on the order of 10⁻¹ Ω cm.

1. Introduction

Thin films of optically transparent metal oxides with high electrical conductivity have a variety of applications in solar energy conversion systems, optoelectronic devices, electrodes of flat-panel displays and touch panels, selective filters for solar thermal collectors, spectrally selective windows, and thermal reflective and antistatic coatings, and recently in chemical sensors.¹

Due to its remarkable combination of optical and electrical transport properties and chemical stability, tin-doped indium oxide (ITO) is one of the most widely used materials for these applications.² Over the past three decades, the development of a number of vapor-phase deposition techniques for ITO has been stimulated by the

outstanding properties and technological value of its thin films.^{3–9} The deposition of transparent and conductive ITO films has been achieved by reactive sputtering³ or evaporation⁴ of metal alloy targets; by rf,⁵ dc,⁶ or magnetron⁷ sputtering of oxide targets; by electron beam evaporation;⁸ and by CVD techniques.⁹ DC-magnetron sputtering systems have now been scaled up for production of commercial quantities of ITO films.^{1b} Although vapor-phase methods can produce high quality ITO films, they have practical disadvantages of high energy consumption, expensive equipment, and poor target utilization.^{1b}

The application of ITO in the next generation of photovoltaic and optoelectronic devices and in photoelectrochemical energy production systems has stimulated interest in the development of new methods for depositing films over large areas. Low-cost solution-based techniques can fulfill these requirements particularly well. There are also applications, including deposition of transparent conductors in high aspect ratio channels and trenches, in which solution-based methods can be more effective than line-of-sight vapor-phase deposition. So far, sol–gel based deposition procedures have received the most attention.^{10–17} These methods, however, rely on a multi-step synthetic protocol that includes colloidal sol preparation followed by spin-^{10,11} or dip-coating^{12–17} and

*Corresponding authors. E-mail: N.I.K., nina@chem.psu.edu; T.E.M., tem5@psu.edu.

- (1) (a) Ginley, D.; Bright, C. *MRS Bull.* **2000**, 25(8), 15. (b) Lewis, B.; Paine, D. *MRS Bull.* **2000**, 25(8), 22. (c) Minami, T. *MRS Bull.* **2000**, 25(8), 38. (d) Patel, N.; Makhija, K.; Panchal, C. *Sens. Actuators, B: Chem.* **1994**, 21, 193. (e) Sberveglieri, G.; Faglia, G.; Groppelli, S.; Nelli, P. *Sens. Actuators, B: Chem.* **1992**, 8, 79. (f) Galkidas, A.; Marthunas, Z.; Setkus, A. *Sens. Actuators, B: Chem.* **1992**, 7, 633.
- (2) (a) Edwards, P.; Porch, A.; Jones, M.; Morgam, D.; Perks, R. *Dalton Trans.* **2004**, 2995. (b) Vossen, J. L. In *Physics of Thin Films* **1977**, 9, 1. (c) Haacke, J. *Annu. Rev. Mater. Sci.* **1977**, 7, 73.
- (3) Lehman, H.; Widmer, R. *Thin Solid Films* **1975**, 27, 359.
- (4) (a) Nath, P.; Bunshah, R. *Thin Solid Films* **1980**, 69, 63. (b) Nath, P.; Bunshah, R.; Basol, B.; Staffsud, O. *Thin Solid Films* **1980**, 72, 463.
- (5) Vossen, J. L.; Poliniak, E. *Thin Solid Films* **1972**, 13, 281.
- (6) Fraser, D.; Cook, H. J. *Electrochem. Soc.* **1972**, 119, 1368.
- (7) Buchanan, M.; Webb, J.; Williams, D. *Appl. Phys. Lett.* **1980**, 37, 213.

- (8) Hjortsberg, A.; Hamberg, I.; Granqvist, C. *Thin Solid Films* **1982**, 90, 323.
- (9) Kane, J.; Schweitzer, H.; Kern, W. *Thin Solid Films* **1975**, 29, 155.
- (10) Kim, S.-S.; Choi, S.-Y.; Park, C.-G.; Jin, H.-W. *Thin Solid Films* **1999**, 347, 155.

thermal processing of the liquid film. These methods often require multiple coating-drying steps to achieve good crystal quality and useful thicknesses.^{10,13,15,17}

Electrochemical deposition of solid metal oxide films is a technologically simple process that can be performed in one step, usually from aqueous solutions.¹⁸ In general, electrochemical deposition of metal oxide films can be performed in three ways:

- (i) Anodic oxidation of metal substrates (e.g., Al, Ti, Zr, Cu, Fe, Ni). This process involves ion diffusion through the film and, therefore, puts limitations on the film structure and thickness.
- (ii) Electrochemical change in the oxidation state of the metal precursors in order to convert them from soluble to insoluble species. These reactions can run at the anode (e.g., for NiO, Fe₂O₃, MnO₂, and CoO₂) or at the cathode (e.g., for Cu₂O). The preparation of films of complex binary metal oxides, e.g. LaMnO₃ and Pb₈Tl₅O₂₄, has also been demonstrated.
- (iii) Electrochemically assisted deposition (EAD) techniques that differ from direct reduction or oxidation in that they exploit electrochemical reactions for altering chemical conditions, such as pH, in the interfacial solution/electrode zone. This causes precipitation in the vicinity of the electrode surface.^{19–29} Because there is no direct electron transfer between metal precursors and the growing electrode film, EAD is applicable to the deposition of insulating and poorly conducting materials. On the other hand, EAD inherits many advantages of direct electroplating, such as applicability to extended, complex shapes and porous substrates, precise localization of the deposit and compatibility with surface patterning, high deposition

rates, and control of thickness and morphology of the deposits by adjusting electrochemical parameters.

Although other reactions may be possible, most protocols described in the EAD literature rely on the reduction of NO₃⁻,^{19–23} H₂O,^{20a} H₂O₂,²⁴ or dissolved O₂²⁵ to produce hydroxide anions or on the oxidation of tartrate or ascorbate anions to produce protons.^{20b,c} Hydroxide can react directly with metal ions to give hydroxide or oxide precipitates or increase the pH in the interfacial zone, which lowers the solubility of preformed colloidal species.²⁶

To date, the EAD method has been successfully used for preparing a number of simple single-component oxide and hydroxide films, such as Cd(OH)₂¹⁹ and Ni(OH)₂²¹ electrodes, ceramic ZrO₂ and CeO₂ films,^{20a} and semiconductor CuO,^{20b} TiO₂,²² and ZnO^{20c,23,25} films. Among these, ZnO films have been studied in the most detail because of their optical properties and the tendency of ZnO to grow as structured films of relatively large single crystals, including nanowire arrays.^{27–29}

This paper describes a first attempt at the electrochemically assisted deposition (EAD) of ITO films. Our interest in this process has been stimulated by both fundamental and practical issues. First, we would like to explore the possibility of applying EAD to the synthesis of more complex binary and doped metal oxide films. As a solution technique, EAD allows one to change composition by adjusting the concentrations of soluble precursors. Precise control over the film composition is crucial for preparing doped metal oxides with desired properties. ITO films, with their interrelated optical and electrical properties that strongly depend on the Sn/In atomic ratio, are very attractive candidates for deposition by EAD. From the practical point of view, EAD is a technologically simple, inexpensive, and environmentally friendly alternative to vapor-phase and sol-gel based methods for ITO film deposition. Although EAD requires conducting substrates, there are applications—such as filling of porous membranes with transparent conducting oxides—where it may have unique advantages over other techniques.³⁰

Here we show that it is possible to rapidly grow thin crystalline ITO films that are transparent and conductive and that the composition-dependent electrical properties of the films can be controlled by simply altering the composition of the starting solutions.

2. Experimental Section

In a typical synthetic protocol, In(NO₃)₃·xH₂O (99%, Alfa-Aesar) was dissolved in an aqueous solution of 4.6 mM HNO₃ (pH 2.3) with or without 0.1 M supporting electrolyte salt (KNO₃ or NaCl). Deionized water was used in all experiments. Solid SnCl₄·xH₂O (98%, Alfa-Aesar) was then added to this solution. Dissolution of SnCl₄ was very fast, and all solutions remained transparent and stable for a period of

- (11) (a) Ederth, J.; Hesler, P.; Hultaker, A.; Niklasson, G.; Granqvist, C. *Thin Solid Films* **2003**, *445*, 199. (b) Kanehara, M.; Koike, H.; Yoshinaga, T.; Teranishi, T. *J. Am. Chem. Soc.* **2009**, *131*, 17736.
- (12) Maruyama, T.; Kojima, A. *Jpn. J. Appl. Phys.* **1988**, *27*, L1829.
- (13) Takahashi, Y.; Okada, S.; Tahar, R.; Nakano, K.; Ban, T.; Ohya, Y. *J. Non-Cryst. Solids* **1997**, *218*, 129.
- (14) Tahar, R.; Ban, T.; Ohya, Y.; Takahashi, Y. *J. Appl. Phys.* **1998**, *83*, 2139.
- (15) Djaoued, Y.; Phong, V.; Badilescu, S.; Ashrit, P.; Girouard, F.; Truong, V.-V. *Thin Solid Films* **1997**, *293*, 108.
- (16) Nishio, K.; Sei, T.; Tsuchiya, T. *J. Mater. Sci.* **1996**, *31*, 1761.
- (17) Ramanan, S. *Thin Solid Films* **2001**, *389*, 207.
- (18) Brewer, G. *Ceram. Bull.* **1972**, *51*, 216.
- (19) Palanisamy, T.; Kao, Y.; Fritts, D.; Maloy, J. *J. Electrochem. Soc.* **1980**, *127*, 2535.
- (20) (a) Switzer, J. *Am. Ceram. Soc. Bull.* **1987**, *66*, 1521. (b) Poizat, P.; Hung, C.-J.; Nikiforov, M.; Bohannan, E.; Switzer, J. *Electrochem. Solid-State Lett.* **2003**, *6*, C21. (c) Limmer, S.; Kulp, E.; Switzer, J. *Langmuir* **2006**, *22*, 10535.
- (21) Ho, K.-C. *J. Electrochem. Soc.* **1987**, *134*, 52C.
- (22) Natarajan, C.; Nogami, G. *J. Electrochem. Soc.* **1996**, *143*, 1547.
- (23) Izaki, M.; Omi, T. *Appl. Phys. Lett.* **1996**, *68*, 2439.
- (24) Pauporte, T.; Lincot, D. *J. Electrochem. Soc.* **2001**, *148*, C310.
- (25) Peulon, S.; Lincot, D. *Adv. Mater.* **1996**, *8*, 166.
- (26) Minoura, H.; Kajita, T.; Yamaguchi, K.; Takahashi, Y.; Amalnerkar, D. *Chem. Lett.* **1994**, 339.
- (27) Peulon, S.; Lincot, D. *J. Electrochem. Soc.* **1998**, *145*, 864.
- (28) Levi-Clement, C.; Katty, A.; Bastide, S.; Zenia, F.; Mora, I.; Munoz-Sanjose, V. *Physica E* **2002**, *14*, 229.
- (29) Tena-Zaera, R.; Elias, J.; Wang, G.; Levi-Clement, C. *J. Phys. Chem. C* **2007**, *111*, 16706.

- (30) (a) Lai, M.; Martinez, J.; Gratzel, M.; Riley, D. *J. Mater. Chem.* **2006**, *16*, 2843. (b) Lai, M.; Riley, D. *Chem. Mater.* **2006**, *18*, 2233.

weeks (0.1 M KNO_3) or days (0.1 M NaCl). However, in all EAD procedures, freshly prepared (~ 30 min old) solutions were used.

A solution of $\text{In}(\text{NO}_3)_3$ (10 mM) and SnCl_4 (0–4.5 mM) was preheated to 79–80 °C in a water bath and placed into an electrochemical cell equipped with a working Au (Au on glass or Au on Si) or ITO electrode, a Pt counter electrode, and an Ag/AgCl reference electrode. The cell was also preheated in the same water bath. EAD was conducted in the potentiostatic mode at -0.5 V (Au electrodes) or -1.3 V (ITO electrodes) at 79–80 °C. The working electrode was then washed thoroughly with deionized water and dried in an Ar stream. The film thickness was estimated using FESEM cross-sectional images and was found to depend on the deposition time. Typical deposition times for 200–300 nm thick films were 1.5–5 min; however, 5–10 min incubation periods were noticed in some cases. Hydroxide films prepared in this way are referred to hereafter as InSnOH films.

For comparison purposes, EAD films were prepared from 1 mM SnCl_4 solutions in 0.1 M KNO_3 (or NaCl) at pH ~ 1.1 (0.075 M HNO_3). These solutions remain stable long enough to perform the deposition successfully. Highly hydrated tin(IV) oxide can be prepared in this way.^{30a} These films are referred to hereafter as $\text{SnO}_x(\text{OH})_y$ films.

EAD experiments were typically performed in air, with no precautions taken to remove or increase the concentration of oxygen in the solution. Therefore, unless otherwise stated, some amount of dissolved oxygen was always present during the reaction. When oxygen-free conditions were needed, the solution was purged with Ar for 20 min prior to deposition.

Gold substrates were prepared by thermal evaporation of a 200-nm-thick Au film on a glass slide or a Si-wafer. AFM images reveal a polycrystalline gold surface with crystal size in the range 20–80 nm. Before the EAD process, the substrates were cleaned in a UV– O_3 chamber at room temperature for 20 min and washed with water.

To convert InSnOH to ITO, the films were heated in air at 300–350 °C for 30–60 min.³¹ For electrical measurements, films were further heated at 600 °C for 20 min.

Both InSnOH and ITO films were characterized by field emission scanning electron microscopy (FESEM, JEOL 6700F, accelerating voltage 3 kV, gun current 20 μA), transmission UV–visible spectroscopy (HP 8452A), and X-ray diffraction (XRD, Philips X'Pert MPD, Cu $\text{K}\alpha$ radiation). The average size of the InSnOH and ITO crystals was determined from the width-at-half-maximum of the [200] and [222] XRD reflections, respectively, using the Scherrer equation.³²

X-ray photoelectron spectra (XPS) of the films were recorded with a Kratos Analytical Axis Ultra, Al $\text{K}\alpha$ X-ray source. Spectra were calibrated to adventitious carbon at 285.0 eV. Sn/In atomic ratios in the films were calculated from the areas of the Sn $3d_{5/2}$ and In $3d_{5/2}$ peaks acquired in slow scanning mode. All calculations were performed with CASA software (Version 2.3.12Dev9).

Current–voltage characteristics were measured across the film in an Au/ITO/Au device configuration in air at ambient temperature (Keithley 2400 SourceMeter). A small piece of Au foil was placed on top of the film, which had been deposited on a gold substrate. The foil was pressed into the film by using a tungsten tip. The contact area was $\sim 10 \mu\text{m}^2$.

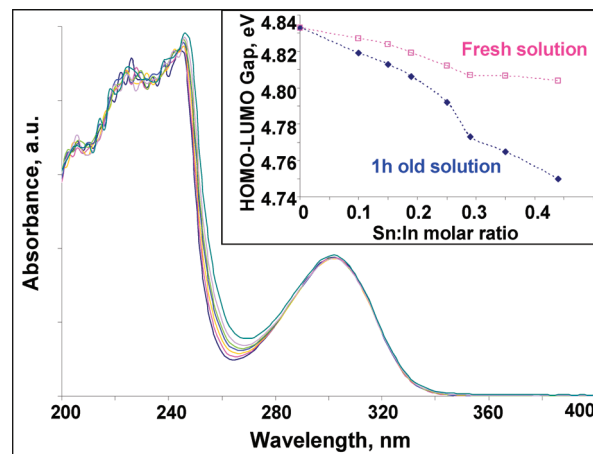


Figure 1. Absorption UV–vis spectra of aqueous solutions of pH 2.3 containing 0.1 M KNO_3 , 10 mM $\text{In}(\text{NO}_3)_3$, and 0–4.5 mM SnCl_4 . (Inset) Dependence of the HOMO–LUMO gap energy of $[\text{In}(\text{H}_2\text{O})_6]^{3+}$ on the Sn/In molar ratio.

3. Results and Discussion

3.1. Film Synthesis: Properties of the Starting $\text{In}(\text{NO}_3)_3$ – SnCl_4 Solutions. It has been established³³ that in aqueous solutions of indium(III) salts that contain noncoordinating anions, such as ClO_4^- or NO_3^- , In^{3+} cations exist as the hexaquo complex, $[\text{In}(\text{H}_2\text{O})_6]^{3+}$. These solutions require acidic conditions to prevent hydrolysis of the complex. In the presence of strongly coordinating Br^- or Cl^- ligands, mixed aquo–halo complexes form. At high $[\text{Cl}^-]/[\text{In}^{3+}]$ ratios, the composition of the mixed complex can be described as $[\text{InCl}_4(\text{H}_2\text{O})_2]^-$ or $[\text{InCl}_5(\text{H}_2\text{O})]^{2-}$.³³ Neutral or weakly acidic aqueous solutions of tin(IV) salts are unstable and hydrolyze to give a white precipitate of hydrous tin(IV) oxide.³⁴

Consistent with these data, in our experiments the dissolution of solid SnCl_4 in a supporting electrolyte solution at pH 2.3 was followed by immediate hydrolysis and the formation of a white precipitate. However, no precipitation of tin species was observed upon SnCl_4 addition to electrolyte solutions that contained previously dissolved $\text{In}(\text{NO}_3)_3$; these solutions remained transparent for a period of weeks. UV–vis spectra of solutions with different $\text{Sn}^{4+}/\text{In}^{3+}$ molar ratios (Figure 1) showed a gradual decrease in the HOMO–LUMO energy gap of the $\text{In}(\text{III})$ complex with increasing Sn^{4+} concentration. This phenomenon became more pronounced in the solutions that were allowed to age for ~ 1 h (see inset in Figure 1).¹¹⁵ In NMR spectra (not shown) revealed significant narrowing of the indium peak in a solution containing tin(IV) species. One of the possible reasons for this narrowing can be a decrease of the ligand exchange rate in the indium aquo complexes in the presence of tin. Although the chemistry of this indium(III)–tin(IV) system requires more thorough investigation, the currently available data suggest the formation of soluble In^{3+} – O – Sn^{4+} complexes.

(31) Sato, T. *J. Therm. Anal. Calorim.* **2005**, *1*, 1–8.

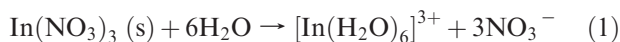
(32) Cullity, B. D. *Elements of X-Ray Diffraction*; Addison-Wesley: Reading, MA, 1978; pp 284–285.

(33) (a) Carty, A.; Tuck, D. *Prog. Inorg. Chem.* **1975**, *19*, 243–337.

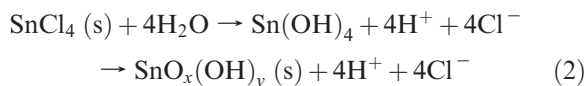
(b) Celeda, J.; Tuck, D. *J. Inorg. Nucl. Chem.* **1974**, *36*, 373. (c) Fratiello, A.; Davis, D.; Schuster, R. *Inorg. Chem.* **1971**, *10*, 1627.

(34) Greenwood, N.; Earnshaw, A. *Chemistry of the Elements*; Butterworth-Heinemann: Oxford, 1998; Chapter 10.

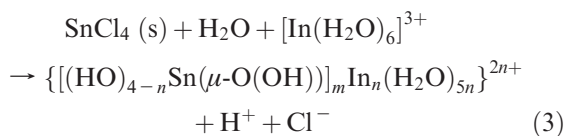
Taking into account the known occurrence of indium germanates in aqueous solutions³⁵ and the rich oxo-cluster chemistry of tin,³⁶ one can infer that $[\text{In}(\text{H}_2\text{O})_6]^{3+}$ cations react with tin species by forming bi- (or poly-) nuclear indium–tin complexes that contain oxo or hydroxo bridges. Thus, chemical transformations in the starting $\text{In}(\text{NO}_3)_3$ – SnCl_4 solutions at pH 2.3 can be tentatively described by the following series of reactions:



In the absence of In^{3+}

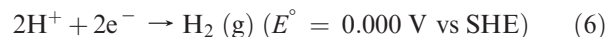
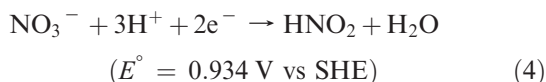


In the presence of excess of In^{3+}



where (s) indicates solid state and n and m may vary as $1 \leq n \leq 4m$ and $m \geq 1$. Such a composition of the soluble indium–tin complex suggests that mono- or polynuclear tin oxo(hydroxo) clusters may replace (or react with) only one water molecule in the coordination sphere of the indium hexaquo complex and that one or more indium aquo complexes may be linked to the tin oxo cluster. This suggestion seems reasonable for solutions with molar ratios $\text{Sn}/\text{In} \ll 1$, which is the case in this study. It should be noted that the solubility and, most likely, the composition of the complexes formed in reaction 3 depend on the In/Sn molar ratio in the solution and the coordinating ability of the anions of the supporting electrolyte. When water or aqueous KNO_3 (0.1 M) were used as supporting electrolytes (pH 2.3), solutions remained transparent up to a molar ratio of $\text{Sn}/\text{In} = 0.45$ (or higher: not studied). When aqueous NaCl (0.1 M, pH 2.3) was used, solutions became cloudy at $\text{Sn}/\text{In} > 0.1$. In NaCl solutions, at ratios of $[\text{Cl}^-]/[\text{In}^{3+}] \geq 10$, mixed indium aquo–chloro complexes can form.³³ Compared to indium hexaquo complexes, the mixed ones have fewer water molecules available for reaction with or replacement by tin species, which may lead to saturation of the solution with tin(IV) at lower Sn/In ratios or the formation of less soluble indium–tin oxo complexes.

Chemistry of the EAD Process. Under the conditions of our experiments, three electrochemical reactions can contribute to a local pH increase in the vicinity of the cathode:



Linear sweep voltammetry (cathodic scans) of Au electrodes measured in KNO_3 and Na_2SO_4 (0.1 M, pH 2.3) solutions with and without dissolved oxygen is presented in Figure 2a–d. In the Na_2SO_4 solution in the absence of oxygen, the onset of cathodic current is at ~ -0.55 V, which indicates the beginning of the H^+ reduction wave (Figure 2d). In the KNO_3 solution in the absence of oxygen, the onset of cathodic current is significantly more positive (~ -0.2 V), and the curve reaches a limiting current maximum at -0.58 V (Figure 2a). Apparently, these parameters characterize the NO_3^- reduction wave. When dissolved oxygen is present, the cathodic curve shows a current increase starting at ~ -0.07 V, the formation of a plateau starting at ~ -0.2 V (Figure 2b*), and a shoulder at ~ -0.45 V on the slope of the NO_3^- reduction wave (Figure 2b). In the absence of NO_3^- anions, the oxygen reduction wave plateaus at ~ -0.45 V (Figure 2c: oxygen-containing 0.1 M Na_2SO_4 solution at pH 2.3). Similar oxygen reduction behavior was observed in oxygen-saturated KCl solutions on a Ni electrode.³⁷ These observations indicate that the reduction of O_2 molecules, NO_3^- anions, and protons can all be used to increase the pH in the vicinity of the cathode. In order to avoid the complication of hydrogen gas evolution on the cathode due to reaction 6, a cathodic potential of -0.5 V was selected for the deposition of InSnOH films on gold substrates. At this potential, the contribution of proton reduction is negligible.

It should be noted that the presence of oxygen leads to a negative shift of the onset and maximum of the NO_3^- reduction wave by ~ 70 mV (Figure 2b, b*). Such a shift may be due to competitive adsorption of intermediate oxygen reduction products (e.g., H_2O_2 and/or HO_2^-) on the Au surface, which can retard electron transfer to NO_3^- anions. Indirect evidence for the formation of an adsorbed layer is the much stronger adhesion of InSnOH films deposited from O_2 -containing solutions. InSnOH film deposition from O_2 -free solutions requires a more negative deposition potential (-0.57 V vs -0.5 V) and results in more weakly adherent films that can be partially washed away during the rinsing step if a water stream is used instead of soaking in water. The maximum of the NO_3^- reduction wave shifts another 100 mV negative when $\text{In}(\text{NO}_3)_3$ (10 mM) and SnCl_4 (1 mM) are present in the O_2 -containing KNO_3 solution (Figure 2e). This indicates partial blocking of the Au surface by formation of the metal hydroxide film.

A cathodic scan of the ITO electrode measured in a KNO_3 (0.1 M, pH 2.3) solution in the presence of dissolved oxygen shows that the reduction of oxygen starts at ~ -0.12 V (vs -0.07 V on Au-cathode) and the

(35) (a) Sarkisov, E.; Lidin, R.; Krymskaya, E. *Inorg. Mater.* **1970**, *6*, 281. (b) Sarkisov, E.; Lidin, R.; Syrkin, V. *Inorg. Mater.* **1971**, *7*, 341.

(36) Davies, G.; Gielen, M.; Panell, K.; Tiekink, E., Eds.; *Tin Chemistry*; Wiley: 2008; pp 69–92.

(37) Jiang, S.; Cui, C.; Tseung, A. *J. Electrochem. Soc.* **1991**, *138*, 3599.

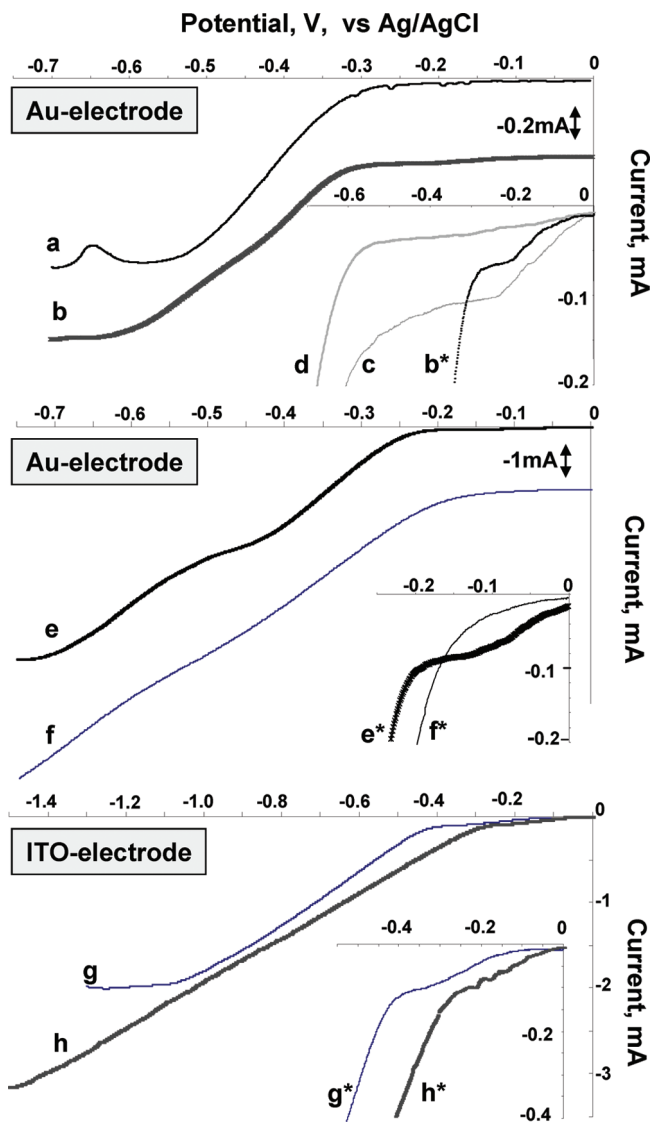
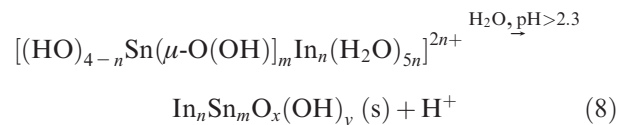
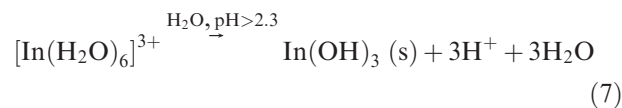


Figure 2. Au and ITO electrode linear sweep voltammetry measured in KNO_3 and Na_2SO_4 solutions of pH 2.3 in the presence and absence (a, d, f) of dissolved oxygen at 78°C . The solution compositions were as follows: (a, b, g) 0.1 M KNO_3 , 4.6 mM HNO_3 ; (c, d) 0.1 M Na_2SO_4 , 2.3 mM H_2SO_4 ; (e, f, h) 0.1 M KNO_3 , 4.6 mM HNO_3 , 10 mM $\text{In}(\text{NO}_3)_3$, and 1 mM SnCl_4 . Solutions a, d, and f were purged with Ar before the EAD process. The sweep rate was 10 mV/s, with reference Ag/AgCl and Pt counter electrodes. The working electrode area was 0.1 cm^2 . The insets show details of the low-current regions.

major cathodic wave plateaus at $\sim -1.1\text{ V}$ (vs -0.65 V at an Au-cathode) (Figure 2g, g*). This suggests higher overpotential on the ITO cathode in KNO_3 solutions compared to the Au cathode. There was no noticeable InSnOH film deposition at -0.5 V , even though the reduction of NO_3^- starts at $\sim -0.4\text{ V}$ (Figure 2g*). The cathodic potential of -1.3 V was thus selected to achieve good deposition of InSnOH films on the ITO cathode.

During EAD processes in neutral solutions, metal hydroxide or oxide films form by direct interaction of metal ions with OH^- ions generated in the cathodic reactions (see e.g. refs 27 and 37). In contrast, in the present case in acidic solutions, metal hydroxide precipitation is a result of hydrolysis reactions that occur because of a pH increase in the vicinity of the cathode.

According to reactions 1 and 3, in $\text{In}(\text{NO}_3)_3\text{-SnCl}_4$ solutions, there are at least two indium and indium–tin complex ions present in solution at the moment the cathodic current begins. Hydrolysis of these ions can be described by eqs 7 and 8:



It is apparent that the composition of the resulting EAD film should be determined by the kinetics of reactions 7 and 8 and by the solubility of the reactions products. Understanding these reactions in detail will require further investigation of the soluble indium–tin oxo-complexes formed in reaction 3, the composition and properties of which may differ significantly in different In–Sn solutions.

3.2. Film Structure and Composition: Scanning Electron Microscopy. Figure 3A, B shows cross-sectional and top views of a InSnOH film deposited on a Au on Si substrate. The EAD film forms a relatively dense and uniform coating on a large (several hundred square micrometers) area of the gold surface. Typical higher resolution FESEM images (Figure 3E, F) reveal that the main feature of the InSnOH films is columnar (70–200 nm in diameter and 100–300-nm-long) bundles of less than 10-nm-thick rodlike crystals. Many of these bundles are oriented almost perpendicular to the electrode surface (Figure 3A). This type of morphology persists in the range of the film Sn/In ratios of 0–0.1 (and possibly higher) for films deposited from 0.1 M KNO_3 or NaCl solutions of pH 2.3 (Figure 3E, F). For comparison purposes, Figure 3C, D shows FESEM images of single-component $\text{In}(\text{OH})_3$ and $\text{SnO}_x(\text{OH})_y$ films deposited on gold substrates from 0.1 M KNO_3 solutions. The $\text{SnO}_x(\text{OH})_y$ film is amorphous and featureless (Figure 3D). In the InSnOH films, this featureless morphology was never found. On the other hand, the morphology of the $\text{In}(\text{OH})_3$ films (Figure 3C) is very close to that of the InSnOH films. It is evident that InSnOH films adopt the morphology of $\text{In}(\text{OH})_3$ and that 1–9% doping by tin atoms does not change it appreciably.

A completely different morphology is observed in the FESEM image of a InSnOH film deposited from a solution (Sn/In = 0.1) that does not contain supporting electrolyte salt. In the absence of KNO_3 or NaCl , the main features of the InSnOH films are flexible sheetlike particles, many of which are oriented nearly perpendicular to the electrode surface (Figure 3G). This suggests that primary InSnOH particles (or seeds) that form in the solution as the pH increases subsequently grow and assemble into either rodlike crystalline bundles or sheetlike

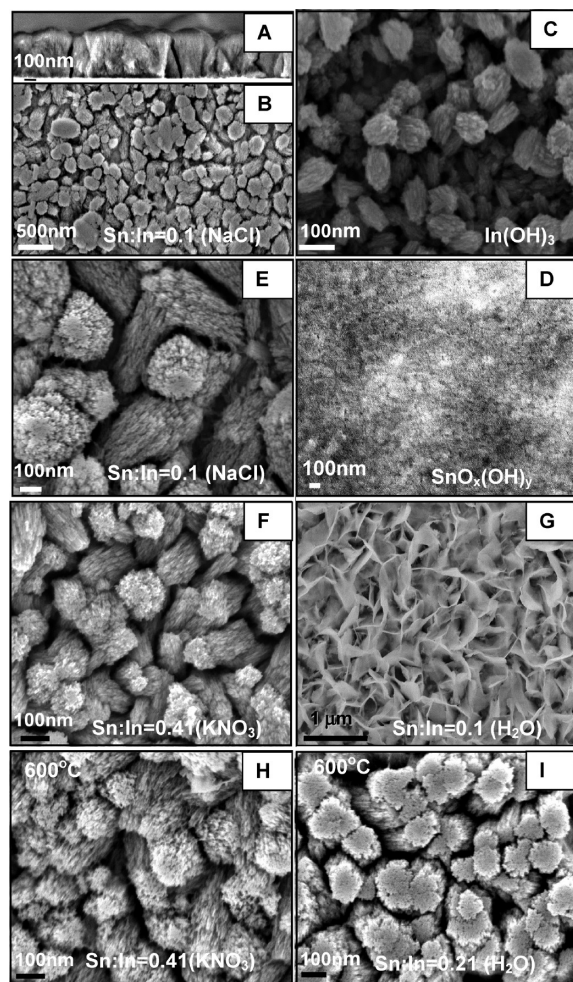


Figure 3. FESEM of the as-prepared InSnOH (A, B, E–G), In(OH)₃ (C), SnO_x(OH)_y (D) films, and InSnOH films heated at 600 °C for 20 min (H, I) deposited on Au-substrates. Deposition solution compositions were as follows: (A, B, E) 0.1 M NaCl, Sn/In = 0.1; (F, H) 0.1 M KNO₃, Sn/In = 0.41; (G, I) H₂O, Sn/In = 0.1 and 0.21 respectively.

particles. The two main differences between solutions with and without the supporting electrolyte are the NO₃[−] ion concentration (134 mM vs 34 mM) and the ionic strength. Taking into account that EAD films deposited from 0.1 M NaCl solutions, which have the same [NO₃[−]] concentration (0.34 mM), do not contain any sheetlike particles, it appears that screening of the surface charge of the primary particles affects the morphology of the film and favors the sheetlike morphology. This picture, however, is not so simple, because at [SnCl₄] ≥ 2 mM in solutions that are free of supporting electrolyte, bundled rods appear to dominate the film morphology. These rods, however, have a more pronounced vertical orientation than in films deposited from KNO₃ solutions (Figure 3I vs H)

Heat treatment of the InSnOH films at 300 °C leads to the dehydration of hydroxide and the formation of oxide (ITO) films. Figure 4A–E shows the gradual transformation of the ITO film morphology with increasing temperature. While heat treatment up to 600 °C does not significantly change the bundle-based morphology of InSnOH films, the ITO rods become thinner and their

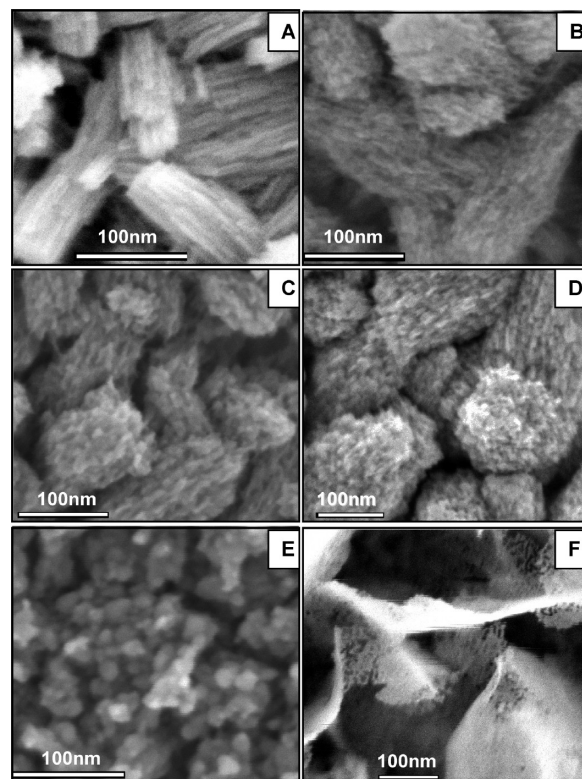


Figure 4. FESEM of heat treated InSnOH films deposited from 0.1 M KNO₃ solution with a Sn/In molar ratio of 0.15: (A) as prepared; (B) 350 °C; (C) 500 °C; (D) 600 °C; (E) 700 °C. (F) film deposited from electrolyte-free solution with a Sn/In molar ratio of 0.1 and heat-treated at 600 °C.

aspect ratio gradually decreases in the temperature range 350 – 600 °C. At 700 °C the rod bundles completely transform into randomly shaped aggregates of roughly spherical nanocrystals (Figure 4E). Heating of the sheetlike particles leads to thinner and rather lacey sheets of the same orientation (Figure 4F). To the best of our knowledge, these morphologies have not been reported for ITO films prepared by other techniques.

X-ray Photoelectron Spectroscopy. The surface Sn content of the InSnOH films was measured by XPS. Taking into account that the films have a relatively uniform morphology with thin (< 10 nm) nanorods as major building blocks (Figures 3 and 4), we suggest that the XPS results obtained for the ~10 nm thick surface layer can represent the composition of the bulk film.

Plots of Sn/In molar ratios in the EAD films versus Sn/In ratios in the deposition solutions are shown in Figure 5A. For solutions containing KNO₃ or no supporting electrolyte, these plots are qualitatively similar (in the range of Sn/In = 0–0.2) and show a noticeable increase in the Sn content of the film for solution ratios of Sn/In ≥ 0.1 (Figure 5A traces 1 and 3). In contrast, in films deposited from NaCl solutions, the Sn content grows almost linearly from the very beginning and drops sharply after the Sn/In ratio in solution reaches 0.1 (Figure 5A, trace 2). At this point, the solutions become saturated with tin and the excess Sn species precipitate due to hydrolysis. The dissimilarity between traces 2 and 3 may be explained by the different properties of the soluble In–Sn complexes

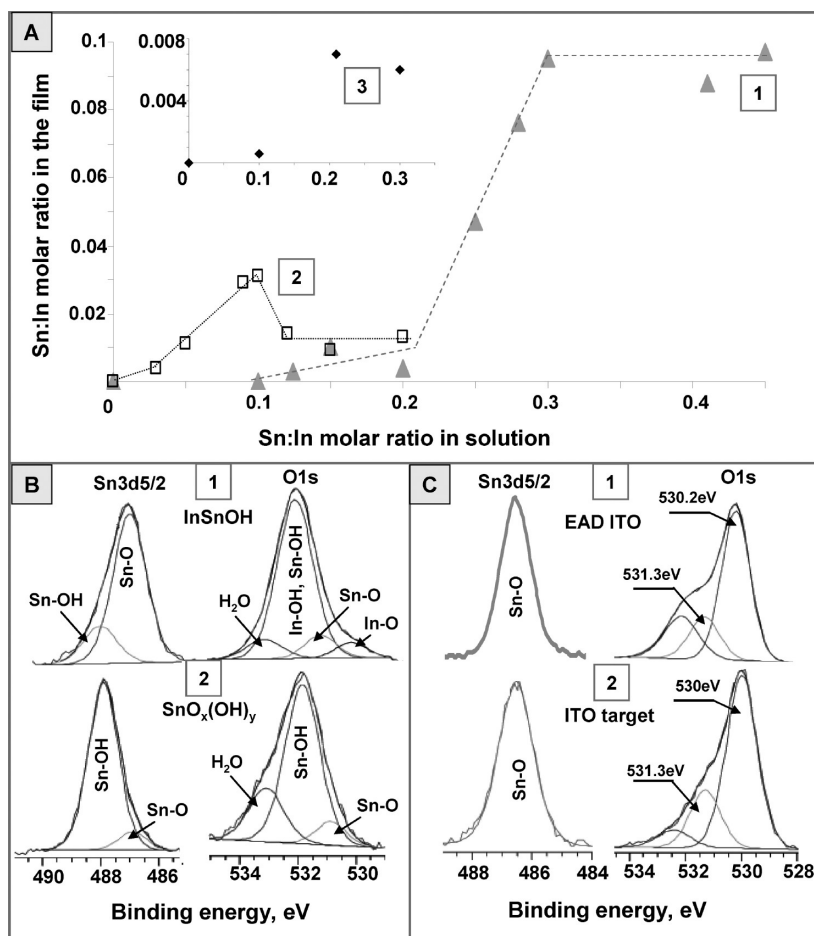


Figure 5. XPS of the EAD films. (A) Dependence of the Sn/In molar ratio in EAD films on the Sn/In molar ratio in solution: (1) 0.1 M KNO₃, 4.6 mM HNO₃; (2) 0.1 M NaCl, 4.6 mM HNO₃; (3) 4.6 mM HNO₃. (B) Sn 3d_{5/2} and O 1s XPS spectra of (1) InSnOH and (2) SnO_x(OH)_y EAD films deposited from 0.1 M KNO₃ solutions: (1) 10 mM In(NO₃)₃, 3 mM SnCl₄, 4.6 mM HNO₃ (pH 2.3); (2) 1 mM SnCl₄, 75 mM HNO₃ (pH 1.1). All bond components were assigned according to. (C) Sn 3d_{5/2} and O 1s XPS spectra of (1) InSnOH EAD film calcined at 600 °C for 1 h and (2) commercial ITO target (Sn/In = 0.09; Kurt Lesker).

that form in solutions containing weakly (NO₃⁻) or strongly (Cl⁻) coordinating anions (see section 3.1).

For films deposited from KNO₃ solutions, the plot area can be divided into four regions (Figure 5A, trace 1). In the first one, as the solution Sn/In ratio increases from 0 to 0.1, there is no detectable Sn in the In(OH)₃ film. In the range of Sn/In ratios 0.1–0.2, the tin content of the film increases, but the increase in Sn/In ratio in the film is slower than that in solution. A break in the graph occurs after the solution Sn/In ratio reaches ~0.2. In the range of Sn/In = 0.2–0.3, the Sn/In ratio in the film grows at the same rate as that in solution (the slope of the plot is ~45°). The film saturates in Sn at a 0.09–0.097 Sn/In ratio, and the graph plateaus in the Sn/In solution range of 0.3–0.45. This plateau, however, is not a result of saturating the solution with tin at [Sn⁴⁺] = 3 mM because there is no noticeable precipitation of tin species as the Sn/In ratio increases from 0.3 to 0.45. Similar behavior was observed in the coprecipitation of indium and germanium hydroxides^{35a} and is considered characteristic of coprecipitation systems that involve chemical interactions between the components.

Comparing this graph with the dependence of the In-(III) HOMO–LUMO gap energy on the solution Sn/In

molar ratio (Figure 1, inset) reveals a certain similarity that may help explain the complex behavior of the indium–tin species during coprecipitation by EAD. In Figure 5A1 at Sn/In = 0–0.2, where the Sn content in the EAD films is low, the HOMO–LUMO gap energy (Figure 1, inset) is relatively constant. The energy decreases in the range of Sn/In = 0.2–0.3 (Figure 1, inset), which corresponds to greater incorporation of Sn in the films (region 3 in Figure 5A1). The decrease in the HOMO–LUMO gap energy slows down (or almost stops) in freshly prepared solutions after the Sn/In ratio reaches ~0.3. This suggests the formation of complexes in solution that maintain their composition as they are incorporated into the film. Tin is thus incorporated into the EAD films as preformed InSnOH compounds and not as islands of a separate hydrated tin oxide phase.

Further evidence for the incorporation of tin from mixed In–Sn complexes comes from comparing Sn 3d_{5/2} and O 1s XPS spectra of films of InSnOH and SnO_x(OH)_y (Figure 5B, traces 1 and 2). The Sn 3d_{5/2} spectrum of the InSnOH film peaks at ~486.9 eV and has a tail at the higher binding energy side (1), whereas the spectrum of the SnO_x(OH)_y film peaks at ~487.8 eV and has a tail at the lower energy side (2). Both of the envelopes, however,

can be fitted with the same Sn–O and Sn–OH bond components³⁸ with a much higher Sn–O to Sn–OH ratio in the InSnOH film. In the O 1s spectra of the InSnOH and SnO_x(OH)_y films, the peak shapes are also different, with peak tails observed at the lower and higher energy sides, respectively. The positions of the peak maxima, however, are about the same (532 ± 0.1 eV) because of the dominant contribution of the metal hydroxide (M = In, Sn) bond component in both films. Both of the envelopes can be fitted to a combination of M–O and M–OH components. The highest binding energy component at ~ 533.1 eV is probably related to bound or occluded water molecules,³⁸ the proportion of which is much lower in the InSnOH film (1) than in the SnO_x(OH)_y film (2). The marked differences in the Sn 3d_{5/2} and O 1s spectra support the conclusion that the InSnOH films do not contain a separate hydrated tin oxide phase.

Figure 5C, traces 1 and 2 compares Sn 3d_{5/2} and O 1s XPS spectra of (1) a InSnOH film calcined at 600 °C and (2) a commercial ITO target powder (Kurt Lesker) taken as a reference. Both Sn 3d_{5/2} spectra are similar and reveal symmetrical peaks at 486.5 and 486.4 eV, which can be fitted with a single Sn–O component. It should be noted that the Sn–O bond energies in SnO and SnO₂ are very close,³⁸ and therefore tin may be present in both Sn⁴⁺ and Sn²⁺ oxidation states, which has been found to be the case in tin-doped indium oxide materials.³⁹

The O 1s spectra in Figure 5C, traces 1 and 2 are also similar, with a maximum at 530.1 ± 0.1 eV and a tail at the high energy side. On the low energy side, one can distinguish two types of O²⁻ anions with a binding energy difference of ~ 1.2 eV. Similar double-oxide peaks have been observed in XPS spectra of sputtered³⁹ and sol-gel derived¹⁰ ITO films. These types of O 1s peaks are characteristic of oxides with metal ions in two or more oxidation states, with the higher binding energy component assigned to O²⁻ ions in oxygen-deficient regions.⁴⁰ Anion deficiency can contribute to doping and thus electrical conductivity in metal oxide films.² Because neither the In 3d_{5/2} nor the Sn 3d_{5/2} spectra show evidence of metal-hydroxide bonds, the third, highest energy (~ 532.4 eV), component in both O 1s spectra is probably related to adventitious carbon-oxygen species. The similarity in the shape of the Sn 3d_{5/2} and O 1s spectra for the EAD ITO film, the sputtered ITO film,³⁹ and commercial ITO powder suggests similar atomic environments of Sn and O atoms in all three materials.

X-ray Diffraction. XRD patterns of the as-deposited In(OH)₃ and InSnOH films are shown in Figure 6A, traces 1 and 2, respectively. All of the films with Sn/In ratios of 0–0.1 can be indexed to cubic In(OH)₃ with a strong preferred orientation in the [100] direction (Figure 6A, traces 1 and 2). The cubic lattice parameters

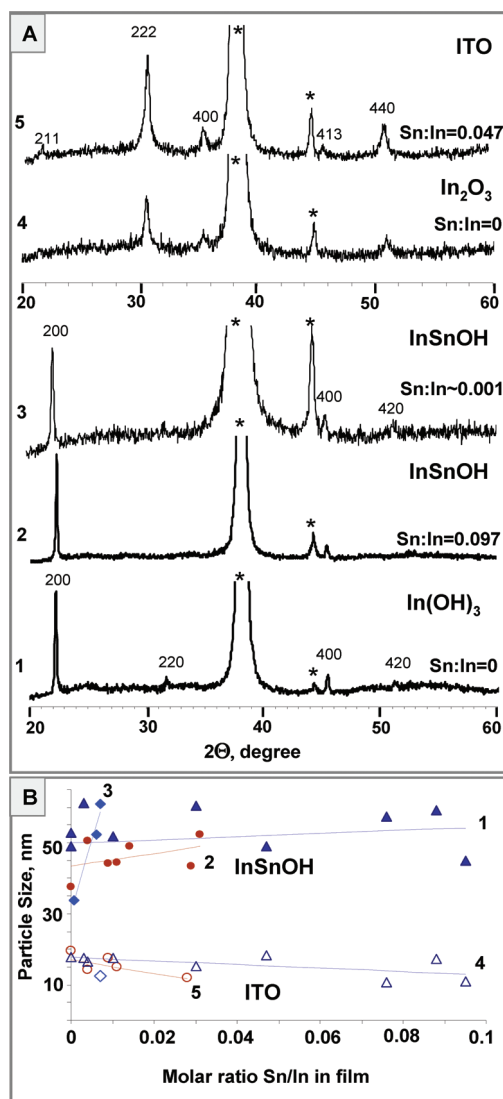


Figure 6. (A) X-ray diffraction patterns of as-prepared (1, 2, 3) and heat-treated at 600 °C (4, 5) films of In(OH)₃ (1, 4) and InSnOH (2, 3, 5) that were deposited from solutions with (1, 2, 4, 5) and without (3) KNO₃ electrolyte. Patterns 2 and 5 are typical for all InSnOH and ITO films, respectively, regardless of the Sn content in the films. (B) Dependence of particle size on the Sn/In atomic ratio in the film for as-prepared (1–3: [200] reflection) and heat-treated at 600 °C (4, 5: [222] reflection) InSnOH films. Lines 1–5 are trend lines. * indicates Au reflections.

fall within the range $a = 7.98 \pm 0.02$, which is in good agreement with reference data ($a = 7.974$ Å).⁴¹ The average particle sizes in the [100] direction are ~ 55 – 45 nm for the films deposited from KNO₃ and NaCl solutions, respectively, with a slight tendency to grow with Sn concentration (Figure 6B, trace 2). Considering these data in relation to the morphology of the films (Figures 3A, E, F and 4A), it appears that the average particle size reflects the length of the mostly vertically oriented thin rods, which align along the [100] direction.

InSnOH films deposited from solutions that do not contain KNO₃ or NaCl show similar XRD patterns with $a = 7.970$ Å and average particle sizes of ~ 50 (Sn/In = 0.006) and ~ 60 nm (Sn/In = 0.007). However, the film

(38) Moulder, J. F.; Stickle, W. F.; Sobol, P. E.; Bomben, K. D. *Handbook of X-ray photoelectron spectroscopy*; Perkin-Elmer Co.: 1992.

(39) Fan, J. C.; Goodenough, J. B. *J. Appl. Phys.* **1977**, *48*, 3524–3531.

(40) Bonnelle, J. P.; Grimblot, J.; D'Huysser, A. *J. Electron Spectrosc. Relat. Phenom.* **1975**, *1*, 151.

(41) ICSD: *The inorganic crystal structure database*; FIZ Karlsruhe & NIST: PC Version Release 2009/2.

with an Sn/In ratio of 0.0007 has a larger unit cell ($a = 8.04 \text{ \AA}$) (Figure 6A, trace 3) and significantly smaller particle size ($\sim 30 \text{ nm}$) (Figure 6B, trace 3). This is the film that is built from sheetlike particles (Figure 3G).

After heat treatment at $350 \text{ }^\circ\text{C}$, all of the films show the cubic crystal structure of In_2O_3 . Further calcination at $600 \text{ }^\circ\text{C}$ in air does not change the crystal structure of the films (Figure 6A, traces 4 and 5). For all of the films, regardless of the Sn/In ratio, the cubic lattice constant is in the range $a = 10.11 \pm 0.01 \text{ \AA}$, and the average particle size in the [111] direction is in the range $10\text{--}20 \text{ nm}$, with a slight tendency to decrease with increasing Sn content in the film (Figure 6B, traces 4 and 5). These data are consistent with FESEM images that show shortening of the rodlike crystals after heat treatment at $600 \text{ }^\circ\text{C}$ (Figure 4A–D). None of the XRD patterns show reflections that can be assigned to tin oxide phases. The XRD patterns of the films are similar to the reference data for ITO samples ($a = 10.12 \text{ \AA}$)⁴¹. Consistent with these results, the XRD patterns of reference ITO samples (Sn:In = 0.03–0.07)⁴¹ and ITO films with Sn content of $\sim 10\%$ ^{3,10} and higher⁴² show no noticeable difference from the patterns of cubic In_2O_3 . Such XRD patterns are associated with SnO_2 present in finely dispersed form.⁴² This suggests that, in the EAD films, tin ions are substitutionally embedded into the In_2O_3 lattice and are not present as a separate phase.

3.3. Optical and Electrical Properties of the Films.

UV–visible transmission spectra of a $\sim 200\text{-nm}$ -thick EAD ITO film (Sn/In = 0.095) deposited on a commercial ITO-glass slide and a FESEM image of the film are shown in Figure 7. The morphology of this film is similar to that of films deposited on Au substrates. Spectra of both the as-prepared InSnOH film (2) and films calcined at $350 \text{ }^\circ\text{C}$ for 30 min (3) follow the ITO-glass spectrum closely (1). Between 340 and 480 nm, the transmittance increases rapidly from 60% to 80%, and it levels off at $\sim 84\%$ in the range 600–800 nm. When visible spectra of the films are recorded against the ITO-glass background (Figure 7, inset), one can see that the as-deposited hydroxide film has a transmission minimum at $\sim 430 \text{ nm}$ that is lower than that of the commercial ITO sample by $\sim 4\%$. After the hydroxide-to-oxide conversion, the transparency of the EAD ITO film improves and becomes $\sim 98\%$ of that of the commercial ITO film. Similar transmittance values were reported for ITO films with about the same tin concentration that were prepared by dc sputtering⁶ and sol–gel methods.^{10,15–17}

The band gap of the EAD ITO film estimated from a UV–vis absorption spectrum (not shown) is 3.88 eV.

Current–voltage (iV) characteristics of the EAD ITO films sandwiched between two gold electrodes reveal two different behavior patterns (Figure 8A inset). About 20% of the films have ohmic iV characteristics (Figure 8A inset, trace 1). However, the majority ($\sim 80\%$) of the Au-ITO-Au structures show reproducible rectifying behavior.

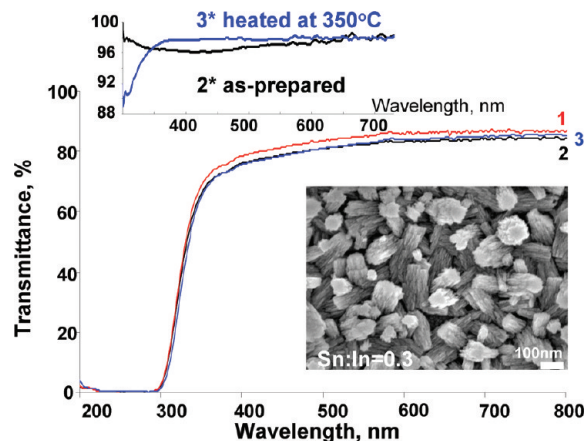


Figure 7. Transmission UV–vis spectra of a commercial ITO-glass slide (1) and as prepared (2) and heat-treated at $350 \text{ }^\circ\text{C}$ for 30 min (3) InSnOH films (200-nm-thick) deposited onto ITO-glass from a 0.1 M KNO_3 solution with a Sn/In ratio = 0.3. (top inset) Visible spectra of the same films recorded against the ITO-glass background. (bottom inset) FESEM image of the InSnOH film on an ITO-glass substrate.

For example, for the film shown in Figure 8A (inset trace 2), the rectification ratio at 2 V is 250. The turn-on potential in the forward bias mode (top Au-electrode negative) is $\sim 0.7 \text{ V}$, which is close to the difference in the work functions of Au and ITO (0.7–1 V). The bottom Au-ITO contact appears to be more resistive, and this may be related to either the formation of a resistive layer at the Au-ITO interface or an increase of the Au cathode work function during the EAD process. This rectifying behavior, although unexpected, is interesting and can in its own right be potentially useful. After the turn-on potential is reached, the resistance drops by several orders of magnitude and the iV characteristic becomes almost linear. The results described below are obtained for this region.

The dependence of the electrical resistance of the EAD ITO films on the molar Sn/In ratio is shown in Figure 8A. One can see that, for films deposited from KNO_3 solutions, the resistance decreases by 2 orders of magnitude with increasing Sn/In ratio in the film from 0 to ~ 0.1 and levels out at Sn/In = 0.09–0.1 (Figure 8A, trace 1). This type of behavior is typical for ITO films prepared by vapor-phase and sol–gel methods, many of which have a minimum in resistivity at 8–10 atom % Sn.^{3,12} The resistivity of 300-nm-thick films with a Sn/In atomic ratio of 0.1 is $\sim 0.9 \text{ } \Omega \text{ cm}$. The resistivity may be slightly lower taking into account the roughness of the ITO films (Figure 3), which makes the real contact area smaller.

It has been established^{2,7} that the conductance of ITO films is associated with shallow donor or impurity states in the proximity of the In_2O_3 conduction band, which are produced by chemical doping of Sn^{4+} for In^{3+} or by the presence of oxygen vacancies in the lattice. The concentration of these states depends on the fraction of tin(IV) ions and on the conditions of deposition and postdeposition annealing of the films. The role of the former is still not completely clear because its optimum values vary from $\sim 6\%$ to $\sim 22\%$ for films prepared by different methods.^{2,6,14} Because the transmittance and conductivity of

(42) Frank, G.; Kostlin, H.; Rabenau, A. *Phys. Status Solidi A* **1979**, *52*, 231.

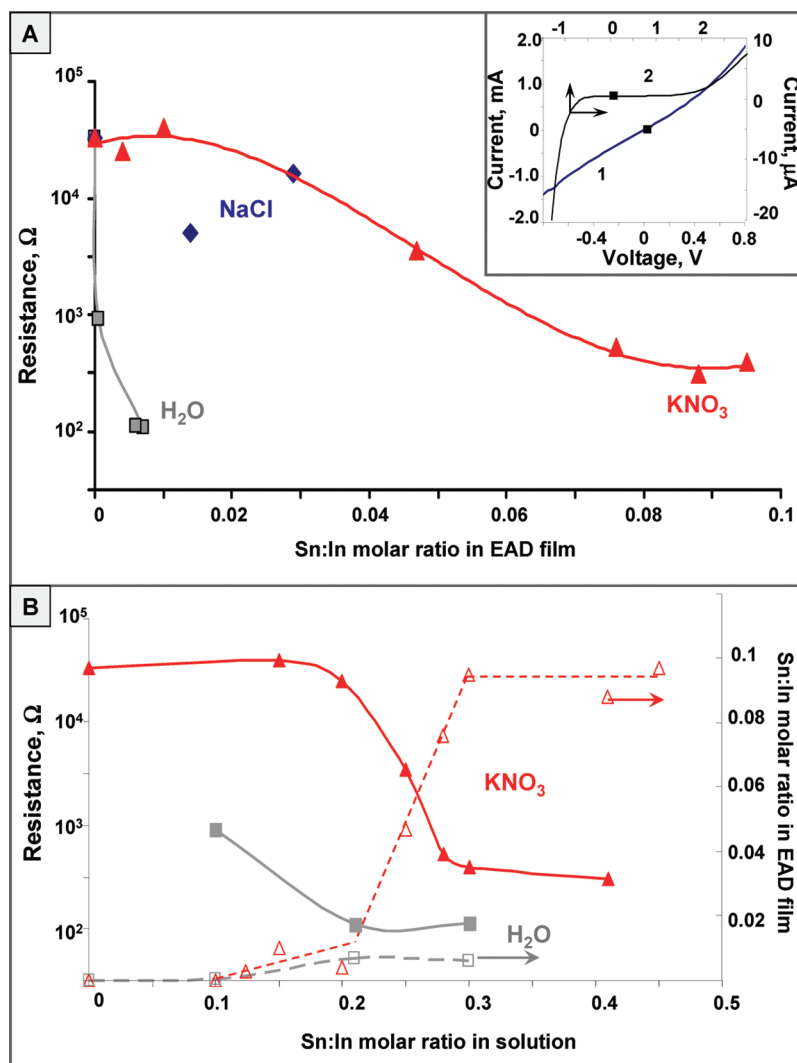


Figure 8. Electrical resistance of EAD ITO (InSnOH calcined at 600 °C for 20 min) films vs (A) Sn/In atomic ratio in the films and (B) Sn/In molar ratio in solution. The electrical measurements were performed across the film in an Au/ITO/Au device configuration. Each resistance value was calculated as the average of five or six measurements for linear regions of the *iV* curves. The part A inset shows two types of *iV* characteristics observed. (B) For comparison purposes, a plot of the Sn/In ratio in the films vs Sn/In ratio in solution is also shown (open dots). The films were deposited from 0.1 M KNO₃ (triangles), 0.1 M NaCl (diamonds), and H₂O (squares) solutions at pH 2.3.

ITO films are interrelated,^{2,43} the parameters of each deposition technique should be adjusted to achieve the required optical and electrical properties for a specific application. Therefore, ITO resistivity data reported in the literature for different deposition techniques vary significantly and fall into the range of 10^2 to 10^{-5} Ω cm.^{4,7,11a,44} Although our EAD ITO films are closer to the upper end of this resistivity scale, we should note that we have not yet attempted to optimize their electrical properties.

In Figure 8B, the film resistance (solid dots) and the film Sn/In ratios (open dots) are plotted versus Sn/In molar ratio in the deposition solutions. One can see a pronounced correlation between decreasing film resistance and increasing Sn content in the film, regardless of the presence or absence of supporting electrolyte. It should be noted, however, that films deposited from the solutions that do not contain supporting electrolyte appear to be much more conductive. These films show

significantly lower resistance at $\sim 10\times$ lower Sn/In ratio than films deposited from KNO₃ solutions (Figure 8A, trace 2). This difference in resistance may originate from the different morphologies of the films. As described in section 3.2, films deposited from the supporting-electrolyte-free solutions contain a larger fraction of the vertically oriented features, either as sheetlike particles (Figure 3G) or rod bundles (Figure 3I vs H).

4. Conclusions

In summary, the electrochemically assisted deposition (EAD) technique has been extended to indium–tin oxides. Thin nanocrystalline tin-doped indium hydroxide (InSnOH) films with variable Sn/In atomic ratio can be synthesized in a fast one-step process from acidic aqueous solutions of mixed In(NO₃)₃ and SnCl₄ precursors. The absence of hydrolysis of tin species in the presence of In³⁺ ions, together with UV–vis and NMR analysis of the solutions, suggests the formation of bi- or polynuclear indium–tin complexes. These precursor complexes favor

(43) Haines, W.; Bube, R. *J. Appl. Phys.* **1978**, *49*, 304.

(44) Vaishnav, V.; Patel, P.; Patel, N. *Thin Solid Films* **2005**, *487*, 277.

the incorporation of tin ions into the crystal lattice of indium hydroxide. Indeed, FESEM, XRD, and XPS data show that, regardless of tin content, all InSnOH films have the morphology and cubic crystal structure of In(OH)₃, and there is no evidence of the presence of a separate tin oxide/hydroxide phase.

Thermal treatment of the as-deposited InSnOH films in air at 300 °C leads to the formation of ITO films with the cubic crystal structure of In₂O₃. XPS analysis suggests a similar chemical structure to ITO materials prepared by vapor phase techniques. The resistivity of the ITO films decreases gradually with increasing tin content and reaches 0.9 Ω cm for an Sn/In atomic ratio of ~0.1. The transmittance of this film is ~84%, which is close to that of ITO films prepared by vapor deposition methods.

The morphology of the EAD ITO films is rather unusual and differs from that of ITO films prepared by other methods. The main structural features of both the InSnOH and ITO films are bundles of < 10-nm-thick rods. According to FESEM and XRD data, these rods are ~50–60-nm-long in the InSnOH films and become about three times shorter after thermal conversion into ITO and heating to 600 °C. Interestingly, when the film structure dominates by the vertically oriented bundles, its resistivity is significantly lower, and it reaches 0.3 Ω cm at Sn/In atomic ratios less than 0.01. This implies that both the Sn content and the bundle orientation in EAD ITO films play a role in conduction. Thus, a route to optimizing the electrical and most likely optical properties of EAD ITO films might be found by increasing the fraction of vertically oriented bundles in the film. Also, optimization of the postdeposition heat treatment procedure (e.g., using N₂ or H₂ enriched atmospheres instead of air^{6,10,43}) remains to be explored.

Films with such bundle-based type of structure should have relatively high surface area and may potentially be useful for applications in chemical sensors, photovoltaic,

photoelectrochemical, and photocatalytic systems. To fully realize the advantages of the EAD synthesis of the transparent and conductive ITO films, the possibility of the film deposition on transparent and nonconductive substrates should be considered. Besides using removable EAD cathodes (such as conductive plastic, or etchable or low melting metals), more sophisticated routes can be envisioned. Because the InSnOH nanocrystals are generated in a solution in the proximity of the electrode (and not at the electrode surface), it may be possible to seed them on a different surface that is located close enough to the electrode. In electrochemical terms, this “proximity of the electrode” may be comparable to the Nernst diffusion layer due to much faster diffusion of the protons that decreases the pH gradient across the diffusion layer. The thickness of the Nernst diffusion layer, in nonstirred systems, is typically ~0.1 mm, so it should be possible to use judiciously engineered substrates containing both conductor and insulator segments. One of the possible scenarios, which is currently under investigation in our lab, is to grow ITO films inside the pores of alumina or polycarbonate membranes to produce ITO nanowires and nanotubes.⁴⁵

Acknowledgment. FESEM and XPS analyses were conducted at the Materials Characterization Laboratory of the Pennsylvania State University. We thank Vince Bojan for acquiring the XPS spectra and helpful discussions. We are grateful to Alan Benesi for acquiring the NMR spectra. This work was supported by the Office of Basic Energy Sciences, Division of Chemical Sciences, Geosciences, and Energy Biosciences, Department of Energy, under Contract DE-FG02-07ER15911.

(45) (a) Kovtyukhova, N.; Mallouk, T. Templated Electrochemically-Assisted Synthesis of Indium Oxide and Indium-Tin Oxide Nanowires, Nanotubes and Their Arrays, *Abstr.*, 2010 MRS Spring Meeting, April 5–9, 2010, San Francisco CA, Q3.10. (b) Kovtyukhova, N.; Mallouk, T. Manuscript to be submitted.